separations

MDPI

Article

Modeling of Adsorption Isotherms of Phenol and Chlorophenols onto Granular Activated Carbon—Part III: Additional Isotherm Formulations and a C_{50}-Normalized Descriptor-Coupled Generalized Model

Oualid Hamdaoui

Chemical Engineering Department, College of Engineering, King Saud University, Riyadh 12372, Saudi Arabia; ohamdaoui@ksu.edu.sa or ohamdaoui@yahoo.fr

Abstract

Related adsorbates are commonly fitted with independent adsorption isotherms, limiting parameter transfer across a chemical family. The equilibrium adsorption of phenol (Ph), 2-chlorophenol (2-CP), 4-chlorophenol (4-CP), 2,4-dichlorophenol (DCP), and 2,4,6-trichlorophenol (TCP) on granular activated carbon (GAC) was re-analyzed to extend the model set evaluated in Parts I and II and to develop a family-level formulation. Five additional equations, Dubinin–Radushkevich (D–R), Flory–Huggins, Harkins–Jura, Halsey, and Henderson, were assessed, primarily by nonlinear regression. D–R gave the best pooled performance among the additional direct isotherm models (RMSE = 7.388 mg/g; APE = 2.718%). The generalized Langmuir/Marczewski–Jaroniec function was then reparameterized exactly using the half-saturation concentration C_{50}. Independent C_{50} values decreased from 34.118 mg/L for Ph to 0.617 mg/L for TCP and were strongly associated with hydrophobicity. A simultaneous descriptor-coupled model constrained C_{50} and the low-concentration exponent from molecular hydrophobicity, reducing adjustable parameters from 20 to 14 while retaining high accuracy for 45 measured observations (RMSE = 4.434 mg/g; APE = 1.600%). Descriptor coupling supports compact correlation within the investigated family; reliable prediction for unseen compounds remains unestablished.

Keywords: granular activated carbon; phenol; chlorophenols; adsorption isotherms; half-saturation concentration; molecular descriptors; nonlinear regression

Check for updates

Academic Editor: Yundong Wang

Received: 22 September 2026
Revised: 14 October 2026
Accepted: 20 October 2026
Published: 21 October 2026

Copyright: © 2026 by the author. Licensee MDPI, Basel, Switzerland. This article is an open access article distributed under the terms and conditions of the Creative Commons Attribution (CC BY) license.

1. Introduction

Adsorption equilibrium modeling is indispensable for interpreting adsorbate–adsorbent interactions and for designing activated-carbon treatment processes. It also presents a recurrent methodological difficulty: many isotherm equations can fit the same dataset well, particularly when additional adjustable parameters are introduced, yet a better numerical fit does not necessarily imply a more informative adsorption model. This issue is especially relevant for heterogeneous carbonaceous adsorbents, for which pore geometry, surface chemistry, solute–solvent interactions, and the molecular properties of the adsorbate simultaneously affect equilibrium uptake [1–3]. Recent methodological studies likewise emphasize nonlinear regression and multi-criterion model selection rather than reliance on linearized forms or a single goodness-of-fit statistic [4,5].

The adsorption of phenol and chlorophenols onto GAC was previously examined in two companion studies. Part I evaluated the Langmuir, Freundlich, Elovich, Temkin, Fowler–Guggenheim, Kiselev, and Hill–de Boer equations and used these models to assess adsorption-energy and lateral-interaction behavior [6]. Part II extended the analysis to thirteen three-, four-, and five-parameter equations, including Redlich–Peterson, Sips, Langmuir–Freundlich, Fritz–Schlunder, Radke–Prausnitz, Toth, Jossens, Weber–van Vliet, and Baudu formulations [7]. The most flexible heterogeneous equations, particularly Baudu, Langmuir–Freundlich, and Sips, represented the data accurately. Because these models have already been developed and discussed in detail in Parts I and II, their equations and theoretical backgrounds are deliberately not repeated in the present work. Selected previously studied models are used only in a final benchmark comparison. Parts I and II examined individual isotherms; Part III assesses additional formulations and descriptor-constrained parameter economy.

Two issues remain scientifically relevant. First, several isotherm formulations based on concepts different from those emphasized previously have not been evaluated for this dataset. The Dubinin–Radushkevich equation is rooted in adsorption-potential and micropore-filling concepts [8,9]. Recent work highlights limitations in applying Flory–Huggins-type expressions to aqueous adsorption data [10]. Harkins–Jura accounts empirically for multilayer adsorption on heterogeneous surfaces [11], whereas Halsey and Henderson equations originate from heterogeneous multilayer adsorption and moisture-sorption descriptions [12,13]. Evaluating these equations provides a useful test of whether alternative physical pictures add explanatory value to the phenol/chlorophenol–GAC system.

Second, all conventional isotherm comparisons treat Ph, 2-CP, 4-CP, DCP, and TCP as independent adsorption systems. Such an approach is effective for interpolation but does not exploit the systematic changes in molecular structure across the homologous series. For the present GAC, the equilibrium uptake increases in the order Ph < 2-CP < 4-CP < DCP < TCP [6]. Across the same sequence, $\log K_{ow}$ increases from 1.46 to 3.69, molecular size increases, aqueous solubility decreases, and acidity generally increases [6]. These systematic trends suggest that part of the apparent variation among individual isotherms should be predictable from molecular descriptors. This premise is consistent with recent quantitative structure–property relationship and machine-learning studies showing that molecular descriptors can support prediction and interpretation of activated-carbon adsorption for organic solutes [14,15].

Recent studies examine regression assumptions and residual validity for dichlorophenol adsorption [16], compare nonlinear isotherms and error criteria for activated-carbon CO_2 adsorption [17], and assess descriptor-based prediction and transfer to unseen compounds [14,15,18]. Half-saturation concentrations are established adsorption parameters [19], with $C_{50} = 1/K$ for Langmuir. The present study uses the established generalized Langmuir/Marczewski–Jaroniec function [20–22] to assess shared descriptor relationships for C_{50} and m. These replace ten compound-specific values with four coefficients, reducing the total parameter count from 20 to 14. The contribution is the assessment of this specific coupling scheme and its parameter economy within the investigated family.

Accordingly, the objectives of this third part are: (i) to evaluate the D–R, Flory–Huggins, Harkins–Jura, Halsey, and Henderson formulations using the original equilibrium database; (ii) to compare these additional models using a consistent nonlinear-regression and information-criterion framework; (iii) to reparameterize an established generalized saturation function exactly through C_{50}; and (iv) to test whether molecular hydrophobicity can replace selected compound-specific parameters in a simultaneous family-level fit. The principal advance is therefore not the proposal of another unconstrained empirical

isotherm, but a reduction in parameter dimensionality that links adsorption affinity and curvature to an adsorbate descriptor while preserving quantitative accuracy.

2. Materials and Methods

2.1. Adsorbent, Adsorbates, and Equilibrium Database

The experimental equilibrium database is identical to that reported in Parts I and II [7]. The adsorbent was a commercial GAC with a BET surface area of 929 m^2/g, a micropore volume of 0.38 cm^3/g, an average pore diameter of approximately 16 Å, a bulk density of 0.45 g/cm^3, an ash content of 5.6%, and a point of zero charge (pH_{PZC}) of 4.1. Before use, the carbon was boiled in ultrapure water, washed to constant conductivity, UV absorbance, and pH, dried at 110 °C to constant mass, and stored in a desiccator.

Five adsorbates were considered: Ph, 2-CP, 4-CP, DCP, and TCP. Equilibrium measurements were carried out at 21 °C using an initial solute concentration of 100 mg/L, variable GAC dose, pH 5.5, and four days of agitation at 400 rpm, which had been verified as sufficient to reach equilibrium. All experiments were performed in triplicate and mean values were reported. The experimental dataset comprises nine measured equilibrium concentration–uptake pairs for each compound (45 in total). The coordinate $C_e = 0$, $q_e = 0$ is a mathematical limiting point, not an experimental measurement [6].

This study is a secondary analysis of the 2007 equilibrium database [6,7]; no new experimental data are presented. All 45 mean concentration–uptake pairs are provided in Table S1. The reported parameters and descriptor relationships are calibrated for the five investigated single-solute aqueous adsorption systems on the specified GAC at 21 °C, pH 5.5, and C_0 = 100 mg/L, within each compound's measured equilibrium concentration range.

Table 1 summarizes the molecular properties relevant to the present descriptor analysis. These values are taken from Part I [6].

Table 1. Molecular properties and experimental maximum adsorption capacities of the investigated phenolic compounds [6].

Property	Ph	2-CP	4-CP	DCP	TCP
Molecular weight, M (g/mol)	94.11	128.56	128.56	163.01	197.45
pK_a	9.9	8.3	9.2	7.7	6.1
Solubility (g/L)	82	22	27	15	0.9
$logK_{ow}$	1.46	2.16	2.39	3.08	3.69
Molecular cross-sectional area, σ (Å^2)	30.49	33.34	33.31	36.77	39.76
Experimental maximum uptake (mg/g)	218	267	310	364	523

2.2. Nonlinear Regression and Statistical Criteria

Wherever an equation provides q_e directly as a function of C_e, parameters were obtained by nonlinear least-squares regression in the original q_e domain. This approach avoids the error redistribution introduced by linearization and permits direct comparison through a common residual definition. The residual sum of squares was

$$SSE = \sum_{i=1}^{N} \left(q_{e,i}^{exp} - q_{e,i}^{pred} \right)^2 \quad (1)$$

Model performance was evaluated using the root-mean-square error,

$$RMSE = \sqrt{\frac{1}{N}\sum_{i=1}^{N}\left(q_{e,i}^{exp} - q_{e,i}^{pred}\right)^2} \quad (2)$$

the mean absolute error,

$$MAE = \frac{1}{N}\sum_{i=1}^{N}\left|q_{e,i}^{exp} - q_{e,i}^{pred}\right| \quad (3)$$

and the average percentage error,

$$APE(\%) = \frac{100}{N^*}\sum_{q_{e,i}^{exp}>0}\left|\frac{q_{e,i}^{exp} - q_{e,i}^{pred}}{q_{e,i}^{exp}}\right| \quad (4)$$

where N = N* = 45 denotes the measured equilibrium pairs, all of which have positive q_e. The five constructed (0, 0) limits are excluded from every regression and fit statistic, including percentage error and information criteria.

Because the central objective is to evaluate parameter economy as well as residual accuracy, the corrected Akaike information criterion and Bayesian information criterion were also used [23,24]:

$$AIC_c = N\ln\left(\frac{SSE}{N}\right) + 2p + \frac{2p(p+1)}{N-p-1} \quad (5)$$

$$BIC = N\ln\left(\frac{SSE}{N}\right) + p\ln N \quad (6)$$

where p is the total number of fitted parameters. Lower values indicate a better compromise between goodness of fit and model complexity. These criteria describe in-sample fit and parameter economy; they do not measure performance for an unseen compound.

Nonlinear regressions were performed using KaleidaGraph 5. Multiple initial parameter sets were used to reduce sensitivity to local minima. Parameters constrained by physical or mathematical requirements were bounded accordingly: $q_m > 0$, $C_{50} > 0$, $0 < m \leq 1$, and $n > 0$; for the extended generalized model, n was not restricted to $n \leq 1$. The reported parameter estimates correspond to the converged least-squares solutions. Logarithmic forms were evaluated only at positive measured equilibrium concentrations. Model curves may be extended to $C_e \to 0^+$ analytically, but the (0, 0) limit was not included as a fitted observation.

Uncertainty and validation calculations were performed with C_e treated as fixed. Local standard errors, approximate 95% profile confidence intervals, parameter correlations, and residual diagnostics were determined for the independent generalized fits and the joint family model. Leave-one-compound-out validation excluded all nine observations of each compound and refitted the global descriptor relationships using the other four compounds. Complete-isotherm prediction used auxiliary log-linear relationships for q_m and n estimated exclusively from those training compounds. Full methods, diagnostic plots, and fold-specific RMSE and APE values are provided in the Supplementary Materials.

3. Additional Isotherm Formulations

Only models not previously developed in Parts I and II are formulated below. Previously published equations are reintroduced solely in Section 5.6 as numerical benchmarks.

3.1. Dubinin–Radushkevich Model

The Dubinin–Radushkevich (D–R) model originates from adsorption-potential theory and was developed for adsorption in microporous solids [8,9]. Its commonly used form is

$$q_e = q_{DR}\exp(-K_{DR}\varepsilon^2) \tag{7}$$

where q_{DR} is a characteristic limiting adsorption capacity, and K_{DR} is related to the characteristic adsorption energy. The Polanyi potential is

$$\varepsilon = RT\ln\left(1+\frac{1}{c_e}\right) \tag{8}$$

where c_e must be dimensionless. In the present calculation,

$$c_e = \frac{C_e\ (\text{mol/ L})}{1\ \text{mol/L}} \tag{9}$$

the characteristic mean adsorption energy is conventionally calculated as

$$E = \frac{1}{\sqrt{2K_{DR}}} \tag{10}$$

The calculated E values are treated here as comparative characteristic-energy descriptors. They are not used as a stand-alone criterion to assign a unique physical or chemical adsorption mechanism, because such interpretation depends strongly on the formulation and units used for ε and K_{DR}.

3.2. Flory–Huggins Model

The following Flory–Huggins-type expression is retained only as a transformed diagnostic because bulk removal fraction and initial concentration do not represent fractional site coverage and equilibrium concentration in the original isotherm [10]. For the fixed initial concentration used in the present experiments, a dimensionless formulation is used with C_{ref} = 1 mg/L:

$$\frac{\theta}{C_0/C_{ref}} = K_{FH}(1-\theta)^{n_{FH}} \tag{11}$$

or

$$\log\left(\frac{\theta}{C_0/C_{ref}}\right) = \log K_{FH} + n_{FH}\log(1-\theta) \tag{12}$$

with

$$\theta = 1-\frac{C_e}{C_0} \tag{13}$$

Here θ is a bulk-solution removal fraction, not a measure of surface coverage or the thermodynamic fractional loading q_e/q_m. Consequently, Flory–Huggins statistics are evaluated on the θ scale and are not directly compared with q_e-space RMSE or AICc values from other models. Throughout Equations (11)–(19), logarithmic arguments involving dimensional quantities are interpreted relative to C_{ref} = 1 mg/L and, where q_e appears inside a logarithm, q_{ref} = 1 mg/g; these unit reference values leave the reported numerical fitting constants unchanged. The transformed Flory–Huggins regression uses only measured data with $0 < C_e < C_0$.

3.3. Harkins–Jura Model

The Harkins–Jura equation is frequently used as an empirical representation of multilayer adsorption on heterogeneous surfaces [11]. It is expressed as

$$\frac{1}{q_e^2} = \frac{B_{HJ}}{A_{HJ}} - \frac{1}{A_{HJ}} \log_{10}\left(\frac{C_e}{C_{ref}}\right) \tag{14}$$

For direct nonlinear fitting in the q_e domain, Equation (14) was rearranged to

$$q_e = \left[\frac{A_{HJ}}{B_{HJ} - \log_{10}(C_e/C_{ref})}\right]^{1/2} \tag{15}$$

within the domain in which the denominator remains positive.

3.4. Halsey Model

The Halsey model was introduced to describe adsorption on nonuniform surfaces [12]. In the form commonly used for liquid-phase adsorption correlations,

$$q_e = \exp\left[\frac{\ln K_H - \ln(C_e/C_{ref})}{n_H}\right] \tag{16}$$

The fitted sign of n_H must be interpreted carefully. For the present increasing aqueous isotherms, unrestricted fitting requires $n_H < 0$. Under that condition, Equation (16) is algebraically equivalent to an increasing two-parameter power law, which explains why its numerical statistics are identical to those of an appropriately parameterized Freundlich equation. The Halsey model is therefore retained as an additional mathematical test but is not assigned an independent multilayer mechanism when the exponent falls outside its conventional interpretation.

3.5. Henderson Model

The Henderson equation was originally developed for equilibrium moisture sorption [13]. Its application to the present liquid-phase adsorption data is therefore empirical. The form adopted in the present analysis can be written as

$$\ln[-\ln(1 - c_e)] = \ln k + n\ln(q_e/q_{ref}) \tag{17}$$

where concentration must be dimensionless and satisfy $0 < c_e < 1$. Because the experimental concentrations are reported in mg/L, direct insertion of raw C_e would be mathematically invalid. The normalized concentration

$$c_e = \frac{C_e}{C_0} \tag{18}$$

was therefore used. Rearrangement gives the direct prediction form

$$q_e = q_{ref}\left[\frac{-\ln(1 - C_e/C_0)}{k}\right]^{1/n} \tag{19}$$

4. Development of the C_{50}-Normalized Descriptor-Coupled Generalized Model

4.1. Generalized Langmuir Mathematical Core

The fractional loading is defined as

$$\theta = \frac{q_e}{q_m} \tag{20}$$

The generalized Langmuir/Marczewski–Jaroniec equation can be written as [20–22]

$$\theta = \frac{(KC_e)^m}{\left[1 + (KC_e)^n\right]^{m/n}} \tag{21}$$

where K sets the concentration scale and m and n control the curvature. In the standard energetic-heterogeneity interpretation, $0 < m \leq 1$ and $0 < n \leq 1$. The mathematical function itself is established; the development below concerns its exact C_{50} reparameterization and descriptor coupling.

For the present dataset, an empirical extension in which $m \leq 1$ was retained but n was allowed to exceed unity provided the most accurate independent representation. Values of $n > 1$ are treated only as empirical transition-shape parameters and are not assigned the standard M–J energy-distribution interpretation.

4.2. Exact Reparameterization Using the Half-Saturation Concentration

Define C_{50} as the equilibrium concentration corresponding to half of the limiting capacity:

$$q_e = \frac{q_m}{2} \qquad \text{at} \qquad C_e = C_{50} \tag{22}$$

Substituting $\theta = 1/2$ and $C_e = C_{50}$ into Equation (21) yields

$$2^{-n/m} = \frac{(KC_{50})^n}{1 + (KC_{50})^n} \tag{23}$$

Hence,

$$(KC_{50})^n = \frac{1}{2^{n/m} - 1} \tag{24}$$

and

$$K = \frac{1}{C_{50}}\left(2^{n/m} - 1\right)^{-1/n} \tag{25}$$

Introducing

$$X = \frac{C_e}{C_{50}} \tag{26}$$

Equation (21) becomes

$$\theta = \frac{X^m}{\left[X^n + \left(2^{n/m} - 1\right)\right]^{m/n}} \tag{27}$$

Therefore,

$$q_e = q_m \frac{(C_e/C_{50})^m}{\left[(C_e/C_{50})^n + \left(2^{n/m} - 1\right)\right]^{m/n}} \tag{28}$$

By construction, $C_e = C_{50}$ gives $q_e = q_m/2$ for any admissible m and n. Thus, C_{50} locates the fitted half-capacity point: a smaller value shifts the normalized isotherm leftward, whereas absolute uptake at a given concentration also depends on q_m, m, and n. This

one-to-one change of variables preserves the isotherm family and leaves the parameter count unchanged.

At high concentration, Equation (28) satisfies $q_e \to q_m$. At sufficiently low concentration,

$$q_e \approx q_m \left(2^{n/m} - 1\right)^{-m/n} \left(\frac{C_e}{C_{50}}\right)^m \tag{29}$$

Consequently, m is the asymptotic log-log slope in the low-concentration region, whereas n primarily controls the sharpness of the transition toward saturation. When $m < 1$, the model does not approach a strict Henry law at the infinite-dilution limit; it should therefore be regarded as a highly accurate finite-range equilibrium correlation unless ultra-dilute data independently establish the limiting behavior.

4.3. Descriptor Coupling

Independent fitting of Equation (28) produces one C_{50} and one m value for each adsorbate. For a family-level formulation, these parameters were related to hydrophobicity because $\log K_{ow}$ changes systematically across the chlorination series and is physically connected with transfer from the aqueous phase to the carbon surface [1,3].

Using a reference concentration $C_{ref} = 1$ mg/L,

$$\ln\left(\frac{C_{50}}{C_{ref}}\right) = \beta_0 + \beta_1 \log K_{ow} \tag{30}$$

A bounded representation was used for m in the final simultaneous fit:

$$m = \frac{1}{1 + \exp[-(\delta_0 + \delta_1 \log K_{ow})]} \tag{31}$$

The limiting capacity q_m and transition parameter n were retained as compound-specific quantities because the five-solute database does not provide sufficiently robust one-descriptor relationships for them. This hierarchy avoids forcing poorly supported correlations merely to reduce the number of parameters.

5. Results and Discussion

5.1. Performance of the Additional Conventional Models

The fitted Dubinin–Radushkevich (D–R), Harkins–Jura, Halsey, and Henderson parameters are summarized in Table 2. D–R gave the lowest pooled error among the four additional models fitted in the adsorption-capacity domain (RMSE = 7.388 mg/g; APE = 2.718%; AICc = 206.5). Halsey had RMSE = 9.014 mg/g but required negative n_H values for all five compounds. Harkins–Jura and Henderson gave larger errors.

The D–R characteristic energy increased overall with chlorination, from approximately 12.3–12.5 kJ/mol for Ph and 2-CP to 20.7 kJ/mol for TCP. This systematic change is compatible with stronger adsorbate–carbon interactions as the molecules become more hydrophobic. Nevertheless, the D–R energy should not be interpreted as an unambiguous mechanistic threshold. Moreover, q_{DR} is an extrapolated characteristic capacity and should not be equated directly with the geometrical monolayer capacities reported in Part I.

Figure 1 compares predicted and experimental q_e values for the four additional models that can be evaluated directly in the q_e domain. D–R and Halsey remain close to the identity line over most of the range, whereas Harkins–Jura shows the largest systematic deviations.

Table 2. Fitted parameters of the additional isotherm models.

Compound	Dubinin–Radushkevich			Harkins–Jura		Halsey		Henderson	
	q_{DR} (mg/g)	K_{DR} (mol²/kJ²)	E (kJ/mol)	A_{HJ}	B_{HJ}	K_H	n_H	k	n
Ph	563.95	3.21876×10^{-3}	12.46	20,891	2.357	1.86679×10^{-6}	−3.270	1.71622×10^{-11}	4.707
2-CP	797.85	3.31034×10^{-3}	12.29	28,458	2.277	4.22546×10^{-6}	−2.987	1.88622×10^{-10}	4.065
4-CP	677.02	2.31234×10^{-3}	14.70	46,199	2.338	8.53990×10^{-9}	−3.975	7.23974×10^{-13}	4.906
DCP	756.80	2.02631×10^{-3}	15.71	70,836	2.368	5.40659×10^{-10}	−4.328	5.67850×10^{-14}	5.185
TCP	814.33	1.17183×10^{-3}	20.66	222,745	2.592	2.53116×10^{-17}	−6.767	4.24835×10^{-18}	6.358

Notes: q_{DR}, Dubinin–Radushkevich characteristic adsorption capacity; K_{DR}, Dubinin–Radushkevich energy constant; $E = (2K_{DR})^{-1/2}$, characteristic mean adsorption energy; A_{HJ} and B_{HJ}, Harkins–Jura constants; K_H and n_H, Halsey parameters; k and n, Henderson parameters. For the D–R model, C_e was converted to molar concentration and the dimensionless concentration was defined relative to 1 mol/L. For the Henderson model, $c_e = C_e/C_0$, with C_0 = 100 mg/L. Negative n_H values were required for all five compounds, and therefore the conventional multilayer interpretation of the Halsey exponent is not applicable to these aqueous adsorption data.

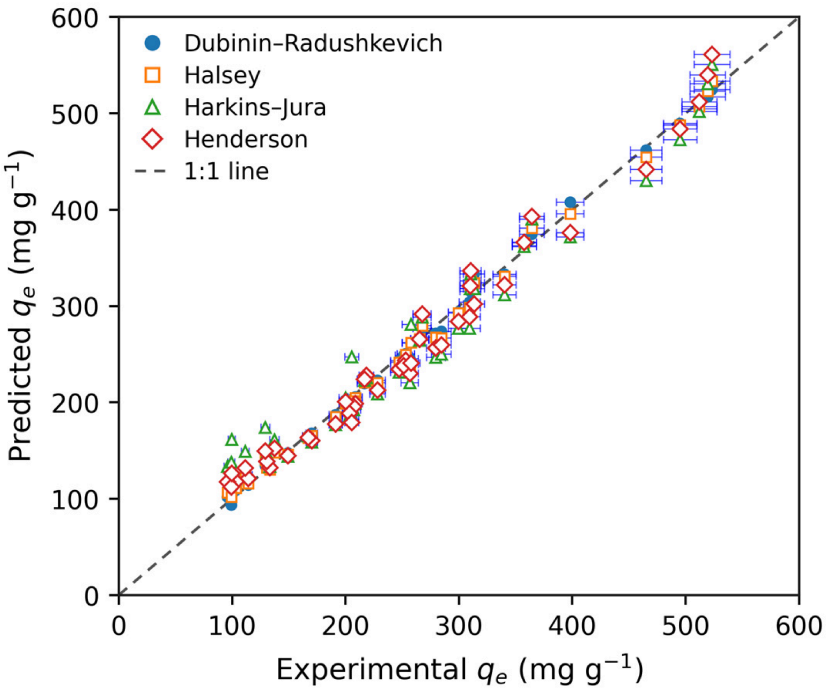


Figure 1. Predicted versus experimental equilibrium adsorption capacities for the additional isotherm models. The dashed line represents perfect agreement. The (0, 0) coordinate, where visible, is a model limit and is not a measured pair. Blue horizontal error bars represent ±3% of the mean experimental uptake obtained from triplicate measurements.

The global statistics are listed in Table 3. The relatively poor Harkins–Jura fit indicates that this particular multilayer/heterogeneous-surface formulation does not provide an adequate quantitative representation of the present equilibrium data; it does not, by itself, exclude multilayer contributions to adsorption. This observation is also consistent with the localized, finite-capacity behavior inferred from Parts I and II [6,7].

Table 3. Pooled fitting statistics for the additional isotherm models (45 measured observations).

Model	Total Fitted Parameters	RMSE (mg/g)	MAE (mg/g)	APE (%)	AIC_c
Dubinin–Radushkevich	10	7.388	5.798	2.718	206.5
Halsey	10	9.014	7.746	3.734	224.4
Henderson	10	17.339	15.104	7.172	283.2
Harkins-Jura	10	24.572	20.530	10.966	314.6

An important mathematical point is that the Halsey form in Equation (16), when n_H is allowed to become negative, reduces to a two-parameter increasing power law. Its fit statistics therefore reproduce those of a Freundlich-type expression. The numerical performance should not be interpreted as independent evidence for a multilayer Halsey mechanism.

5.2. Flory–Huggins Diagnostic Evaluation

Because the initial concentration C_0 was fixed at 100 mg/L and the adsorbent dose varied, the Flory–Huggins form is evaluated only as a transformed diagnostic. Its response is the removal fraction $\theta = 1 - C_e/C_0$ rather than equilibrium uptake q_e. Table 4 lists the transformed parameters; all fitted exponents were negative. This expression is not treated as a predictive q_e isotherm for this dataset.

Table 4. Flory–Huggins parameters for C_0 = 100 mg/L and $\theta = 1 - C_e/C_0$.

Compound	K_{FH} (Diagnostic)	n_{FH} (Diagnostic)	R^2 (Diagnostic)
Ph	0.001791	−0.810	0.783
2-CP	0.002602	−0.537	0.700
4-CP	0.003092	−0.314	0.646
DCP	0.003839	−0.235	0.572
TCP	0.004421	−0.156	0.607

The negative exponents and relatively weak transformed correlations show that this Flory–Huggins transformation has limited descriptive value for the present fixed-initial-concentration data. Because its response is the bulk removal fraction, not true fractional surface loading, its coefficients have no defensible lattice-coverage interpretation. The transformed statistics are therefore reported separately from the q_e-space model comparison.

5.3. Independent Fitting of the C_{50}-Normalized Generalized Model

The C_{50}-normalized generalized equation, Equation (28), represented all five isotherms with high accuracy (Figure 2). The fitted parameters are reported in Table 5. The most striking result is the progressive decrease in C_{50} from 34.118 mg/L for Ph to 0.617 mg/L for TCP. This approximately 55-fold difference in fitted half-capacity concentration reflects a leftward shift of the normalized response across the series.

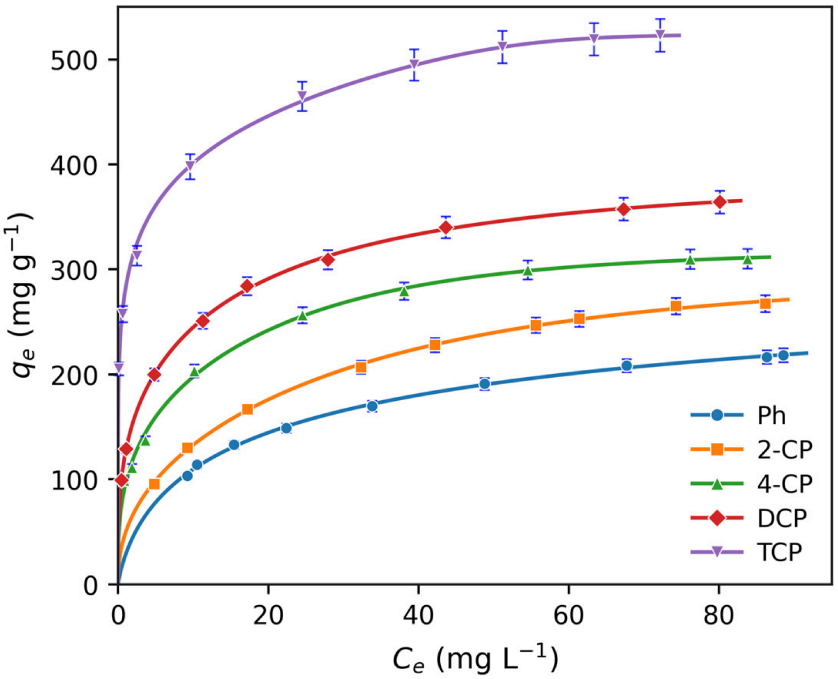


Figure 2. Experimental equilibrium data and independent fits of the C_{50}-normalized generalized model. The (0, 0) point is a constructed model limit, not an experimental measurement. Blue error bars represent ±3% of the mean experimental uptake obtained from triplicate measurements.

Table 5. Parameters of the independently fitted C_{50}-normalized generalized equation. Each fit uses nine measured points.

Compound	q_m (mg/g)	C_{50} (mg/L)	m	n	RMSE (mg/g)	APE (%)
Ph	344.40	34.118	1.000	0.511	1.637	1.048
2-CP	302.30	13.649	0.432	1.814	1.760	0.855
4-CP	321.24	5.112	0.314	2.254	4.538	2.565
DCP	393.29	4.545	0.297	1.435	1.790	0.442
TCP	523.99	0.617	0.153	7.949	5.348	1.245

The fitted values of n exceed unity for several chlorophenols. As noted above, these values lie outside the conventional M–J energetic-heterogeneity domain and must therefore be interpreted as empirical shape parameters. The numerical superiority of this extended form is useful for constructing a family-level descriptor-constrained model, but it does not justify attributing conventional energy-distribution meaning to $n > 1$. The phenol estimate m = 1.000 reached the imposed upper bound; consequently, the relationship involving m should be interpreted cautiously as an exploratory development-set correlation.

Normalization by q_m and C_{50} produces a common half-saturation anchor at (C_e/C_{50}, q_e/q_m) = (1, 0.5) (Figure 3). The curves do not fully collapse because their shape parameters remain compound-dependent; instead, the normalized plot isolates exactly how much variation remains after the principal affinity and capacity scales have been removed.

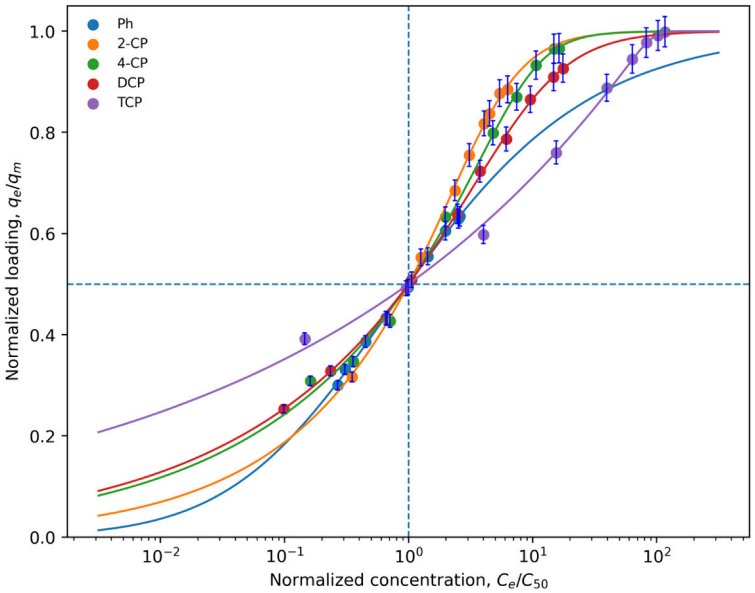


Figure 3. C_{50}-normalized representation of the five adsorption isotherms. Dashed lines indicate the common half-saturation point $C_e/C_{50} = 1$ and $q_e/q_m = 0.5$. Blue bars represent ±3% of the normalized experimental uptake; fitted-parameter uncertainty is excluded.

5.4. Molecular–Property Dependence of C_{50} and Isotherm Curvature

The independently fitted C_{50} values correlate strongly with hydrophobicity. Regression of the five values gives

$$\ln\left(\frac{C_{50}}{1\ \mathrm{mg/L}}\right) = 6.0378 - 1.6732 \log K_{ow}, \qquad R^2 = 0.9194 \tag{32}$$

The negative slope means that increasing hydrophobicity systematically shifts half-saturation to lower aqueous concentration (Figure 4).

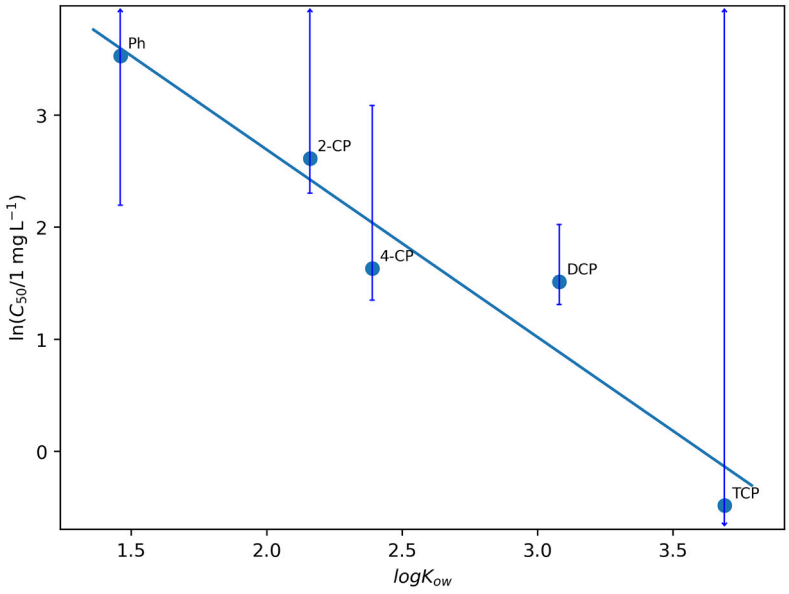


Figure 4. Relationship between independently fitted half-saturation concentration and molecular hydrophobicity. Blue bars show approximate 95% profile confidence intervals (Table S2). Arrows mark bounds beyond the displayed range; the upper C_{50} limit for TCP remains unresolved.

The low-concentration exponent also varies systematically:

$$\ln m = 0.9265 - 0.7606 \log K_{ow}, \qquad R^2 = 0.9141 \tag{33}$$

Thus, chlorination modifies not only the concentration scale of adsorption but also the shape of the low-concentration region (Figure 5).

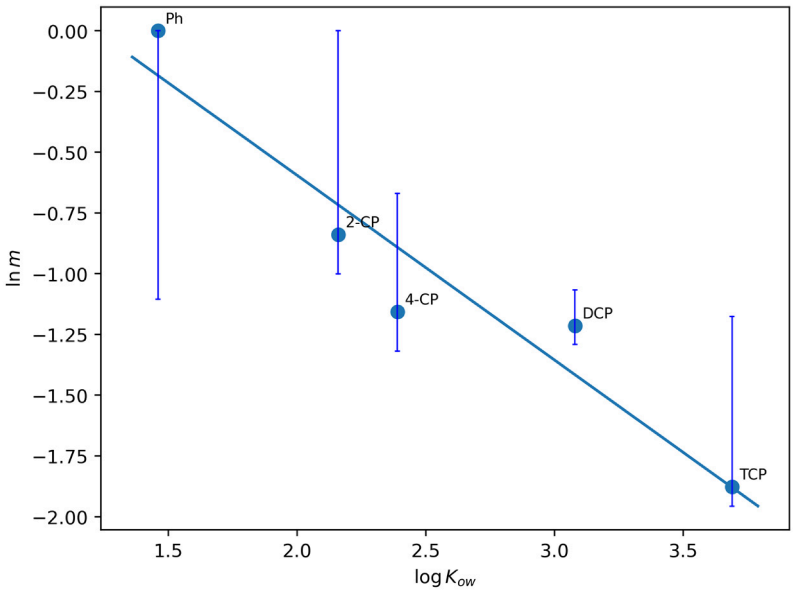


Figure 5. Relationship between the independently fitted low-concentration exponent m and molecular hydrophobicity. Blue bars show approximate 95% profile confidence intervals (Table S2); the upper m limits for Ph and 2-CP reach the imposed boundary.

The relationships in Equations (32) and (33) are physically plausible but must be interpreted as development-set relationships rather than universal quantitative structure–property relations. Only five compounds are available, and molecular weight, chlorination degree, solubility, cross-sectional area, pK_a, and $\log K_{ow}$ are mutually correlated within this homologous series. Introducing several descriptors simultaneously would therefore create severe multicollinearity and an unjustified appearance of predictive precision. Broader descriptor-based studies similarly show that predictive transferability depends on chemical space, adsorbent characteristics, and explicit applicability-domain control [14,15].

5.5. Simultaneous Descriptor-Coupled Family Fit

The central test of the descriptor-coupling concept is whether molecular information can reduce the number of independent fitted parameters without materially degrading accuracy. Accordingly, all 45 measured observations were fitted simultaneously using Equation (28), with C_{50} constrained by Equation (30) and m constrained by the logistic form in Equation (31). The five q_m values and five n values were retained as compound-specific parameters. The resulting model therefore contains 14 parameters: four global descriptor coefficients and ten compound-specific saturation/transition parameters, compared with 20 parameters for five fully independent four-parameter fits.

The optimized global relationships were

$$\ln\left(\frac{C_{50}}{1\ \text{mg/L}}\right) = 7.30071 - 1.92263 \log K_{ow} \tag{34}$$

and

$$m = \frac{1}{1 + \exp[-(2.98206 - 1.26893 \log K_{ow})]} \tag{35}$$

Table 6 lists the compound-specific parameters and the C_{50} and m values constrained by the global descriptor equations.

Table 6. Parameters of the simultaneous 14-parameter descriptor-coupled family model.

Compound	q_m (mg/g)	n	Descriptor-Constrained C_{50} (mg/L)	Descriptor-Constrained m
Ph	441.21	0.407	89.449	0.756
2-CP	375.27	0.813	23.285	0.560
4-CP	449.02	0.508	14.964	0.487
DCP	377.37	1.989	3.971	0.284
TCP	582.24	1.817	1.229	0.154

The simultaneous family fit gave

$$\text{RMSE} = 4.434 \text{ mg/g; APE} = 1.600\% \quad (36)$$

The corresponding information criteria were AICc = 176.0 and BIC = 187.3. Figure 6 shows close agreement for the 45 measured pairs. The (0, 0) limit has not contributed to these statistics.

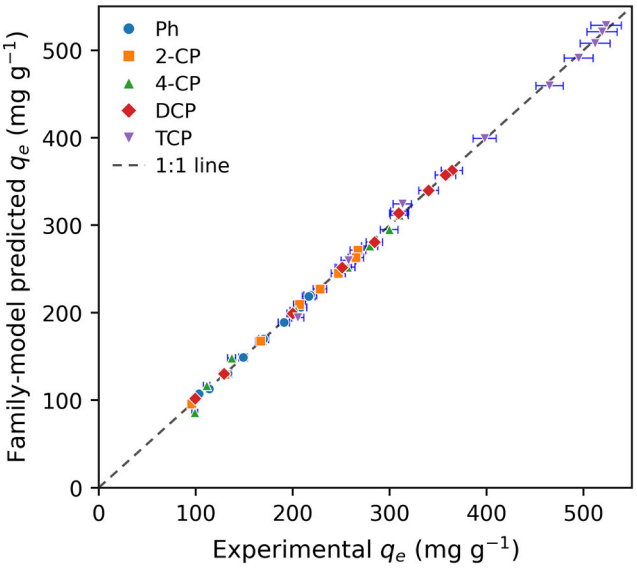


Figure 6. Experimental versus model-calculated adsorption capacities for the simultaneous 14-parameter descriptor-coupled family model. The dashed line is the 1:1 line. A plotted (0, 0) coordinate denotes the model limit and is not an experimental observation. Blue horizontal error bars represent ±3% of the mean experimental uptake obtained from triplicate measurements.

The uncertainty analysis indicates weak identification of several parameters (Tables S2–S5), while residual dispersion differs among compounds (Figures S1–S3). The training-only extension evaluated by leave-one-compound-out validation gave a pooled RMSE of 57.093 mg/g and APE of 20.289%, with individual-compound results reported in Table S6. These findings support cautious parameter interpretation and restrict the contribution to compact correlation of the measured family; reliable prediction of complete isotherms for unseen compounds has not been established.

The descriptor-coupled values of C_{50} differ from the independently fitted values in Table 5 because the simultaneous regression optimizes all global and compound-specific parameters together. This distinction is important. Equations (32) and (33) de-

scribe exploratory relationships derived from the independently fitted isotherms, whereas Equations (34) and (35) define the descriptor relationships obtained by simultaneous global regression and should be used only for interpolation and parameterization within the present fitted family.

5.6. Benchmark Against Models Previously Treated in Parts I and II

To preserve the scope of this third paper, the theoretical derivations of models already published in Parts I and II are not repeated. Selected previous equations were refitted by the same nonlinear least-squares protocol solely to provide a fair benchmark against the newly evaluated and developed formulations. Table 7 summarizes the pooled statistics.

Table 7. Global benchmark of the present models against selected isotherms previously treated in Parts I and II. All fit statistics use 45 measured equilibrium pairs; the origin is excluded. Here, p is the total fitted parameter count.

Model	Status in Present Paper	p	RMSE (mg/g)	APE (%)	AIC_c	BIC
Descriptor-coupled C_{50} family model	Proposed in Part III	14	4.434	1.600	176.0	187.3
Independent extended generalized model	Part III mathematical benchmark	20	3.411	1.231	185.4	186.6
Sips/Langmuir–Freundlich	Part II benchmark	15	4.951	1.780	190.5	201.1
Standard generalized Langmuir (M–J domain)	Part III theoretical benchmark	20	4.175	1.460	203.6	204.8
Baudu	Part II benchmark	20	4.345	1.443	207.2	208.3
Dubinin–Radushkevich	Additional model, Part III	10	7.388	2.718	206.5	218.1
Toth	Part II benchmark	15	6.664	2.166	217.3	227.8
Halsey	Additional model, Part III	10	9.014	3.734	224.4	236.0
Freundlich	Part I benchmark	10	9.014	3.734	224.4	236.0
Henderson	Additional model, Part III	10	17.339	7.172	283.2	294.8
Harkins–Jura	Additional model, Part III	10	24.572	10.966	314.6	326.2
Langmuir	Part I benchmark	10	33.802	9.416	343.3	354.9

The independent extended generalized model gave the lowest residual error (RMSE = 3.411 mg/g) with 20 fitted parameters. The 14-parameter descriptor-coupled model gave RMSE = 4.434 mg/g. AICc favored the reduced model (176.0 versus 185.4; ΔAICc $\approx$ 9.4), whereas BIC weakly favored the independent model (186.6 versus 187.3; ΔBIC $\approx$ 0.8). The reduced model therefore provides parameter economy with a modest loss of in-sample fit. The compound-level validation also indicates limited predictive transferability (Table S6).

The benchmark also shows that the new D–R analysis, while physically informative, does not outperform the best heterogeneous saturation equations from Part II. This is an important result because it demonstrates the value of Part III without artificially portraying every additional model as superior. The advance assessed here is the reduction of independently adjustable parameters through shared molecular-descriptor relationships.

5.7. Physical Interpretation and Limitations

The weak Harkins–Jura fit and the transformed Flory–Huggins diagnostic limit the utility of those specific expressions for these data; neither result establishes whether multilayer adsorption occurs. The D–R model provides a reasonable empirical description, consistent with a microporous adsorbent. Its characteristic capacity and energy are model-dependent and should not be equated with monolayer capacity or used alone to classify adsorption as physical or chemical.

Equation (21) gives $1 - \theta \sim (m/n)(KC_e)^{-n}$ as $C_e \to \infty$; hence $n > 1$ implies an approach to saturation faster than Langmuir. For a local Langmuir site with affinity b, $C_e(1 - \theta_l) = C_e/(1 + bC_e)$ is increasing; this property is preserved by any concentration-independent, nonnegative mixture of such sites. The $n > 1$ extension is therefore incompatible with the standard M–J energy-distribution interpretation [21], although it remains bounded and monotone. Lateral interactions or coverage-dependent affinity could motivate a different theoretical description, but $n > 1$ alone does not establish either mechanism, especially given the finite concentration range and the uncertainty of the fitted parameters.

Third, and most importantly, the large systematic variation in C_{50} across the phenolic series captures the effect of molecular structure more transparently than conventional affinity constants. The C_{50} values obtained from independent fits decrease from 34.12 to 0.617 mg/L as $\log K_{ow}$ increases from 1.46 to 3.69. This trend is consistent with the increasing tendency of chlorinated phenols to leave the aqueous phase and interact with the aromatic carbon surface. The descriptor relationship should nevertheless be regarded as a family-level prototype because only five compounds are presently available. The use of $\log K_{ow}$ as the sole descriptor should also be interpreted in light of acid–base speciation. At the experimental pH of 5.5, ionization is expected to be most relevant for TCP (pKa = 6.1), so neutral-species hydrophobicity cannot by itself represent all solution-phase effects.

The current model also deliberately leaves q_m and n compound-specific. Leaving them compound-specific avoids imposing unsupported descriptor relationships, although the remaining fitted parameters still carry a risk of overfitting. The five solutes are insufficient to determine whether capacity is controlled predominantly by molecular cross-sectional area, micropore accessibility, orientation, or another descriptor, and the fitted n values show nonmonotonic behavior. A larger database should include substituted phenols that decouple hydrophobicity, acidity, steric size, and substitution pattern. The compound-level test indicates that larger datasets are needed to establish transferable relationships for q_m and n, consistent with recent compound-grouped validation findings [18].

Finally, the descriptor-coupled model is not intended to replace thermodynamically rigorous infinite-dilution treatment. Because several fitted m values are below unity, the low-concentration asymptote follows a power law rather than Henry behavior. The model should therefore be regarded as a highly accurate finite-range equilibrium correlation and as a framework for molecular–property coupling over the concentration domain represented by the experimental data.

Because q_m and n remain compound-specific, the present formulation is not yet a fully structure-based predictive model for an unseen adsorbate. Rather, it is a descriptor-constrained family-level equilibrium model in which two of the four compound-dependent parameters are replaced by molecular–property relationships. Prediction of a complete

isotherm for a new compound without equilibrium fitting will require transferable relationships for q_m and n, followed by external validation on a broader range of substituted phenols excluded from model calibration.

6. Conclusions

This third-stage analysis examined five additional formulations for the phenol/chlorophenol–GAC equilibrium data. Among the four models fitted directly in the q_e domain, D–R gave the lowest pooled error (RMSE = 7.388 mg/g; APE = 2.718%). Harkins–Jura and Henderson were less accurate. The Flory–Huggins transformation gave negative exponents and modest transformed correlations, while Halsey required negative exponents and reduced to an increasing power law, limiting the mechanistic interpretation of either formulation.

The principal contribution of Part III is the assessment of descriptor-constrained parameter reduction using an established generalized adsorption function expressed through the conventional half-saturation concentration C_{50}. This parameter defines a transparent fitted half-capacity concentration scale and revealed a pronounced decrease from 34.118 mg/L for phenol to 0.617 mg/L for TCP. In the five-compound development set, C_{50} and m showed high correlations with $\log K_{ow}$ (R^2 = 0.9194 and 0.9141, respectively).

In a simultaneous fit to 45 measured equilibrium pairs, the descriptor-coupled family model reduced the adjustable parameter count from 20 to 14 and gave RMSE = 4.434 mg/g and APE = 1.600%. AICc favored the reduced model (176.0 versus 185.4), whereas BIC was slightly lower for the independent 20-parameter model (186.6 versus 187.3). C_{50} normalization and molecular-descriptor coupling thus provide a compact family-level correlation. Because q_m and n remain compound-specific and only five related compounds were studied, the formulation requires broader external validation before it can be used to predict complete isotherms for new adsorbates.

Supplementary Materials: The following supporting information can be downloaded at: https://www.mdpi.com/article/10.3390/separations13100305/s1, Table S1: All 45 mean equilibrium pairs reused from Parts I and II. C_e: mg/L; q_e: mg/g; Table S2: Independent four-parameter generalized fits. Confidence limits are approximate 95% profile limits; Table S3: Joint parameter estimates, local SEs, and approximate 95% profile limits for the family model; Table S4: Complete local correlation matrix for the 14-parameter family model; Table S5: Complete local correlations for each independent generalized fit; Table S6: Prediction errors for complete excluded isotherms using the training-only extension; Figure S1: Residuals (observed minus fitted q_e) against C_e. Colored circles: family model; gray crosses: independent fits. Panels use separate residual scales; Figure S2: Pooled normal Q–Q plots for independent and family residuals. Reference lines fit the normal quantiles; tail departures caution against assuming normally distributed errors; Figure S3: Residuals against fitted uptake for both models. Panel-specific scales show that residual dispersion differs among compounds.

Funding: The author gratefully acknowledges the financial support provided by the Ongoing Research Funding Program (ORF-2026-2128), King Saud University, Riyadh, Saudi Arabia.

Data Availability Statement: Data are contained within the article or Supplementary Materials.

Conflicts of Interest: The author declares no conflicts of interest.

Nomenclature

The symbols used in this manuscript are defined below:

A_{HJ}, B_{HJ}	Harkins–Jura constants
C_0	Initial adsorbate concentration (mg/L)
C_{ref}	Reference concentration (1 mg/L)

C_e	Equilibrium adsorbate concentration (mg/L)
C_{50}	Equilibrium concentration at $q_e = q_m/2$ (mg/L)
c_e	Dimensionless concentration (defined separately in Equations (9) and (18))
E	D–R characteristic mean adsorption energy (kJ/mol)
K_{DR}	Dubinin–Radushkevich energy constant (mol^2/kJ^2)
K_{FH}	Dimensionless Flory–Huggins diagnostic coefficient
n_{FH}	Flory–Huggins exponent
K_H	Dimensionless Halsey constant
k	Dimensionless Henderson constant
K	Generalized-isotherm affinity scale (L/mg)
m,n	Generalized-isotherm shape exponents
N	Number of measured equilibrium pairs (45 pooled)
p	Number of fitted parameters
q_e	Equilibrium adsorption capacity (mg/g)
q_{ref}	Reference adsorption capacity (1 mg/g)
q_m	Limiting adsorption capacity (mg/g)
q_{DR}	D–R characteristic adsorption capacity (mg/g)
R	Universal gas constant (0.0083144626 kJ/mol K)
T	Absolute temperature (K)
X	Dimensionless concentration, C_e/C_{50}
θ	Fractional loading (generalized model) or bulk-solution removal fraction (Flory–Huggins diagnostic)
ε	Polanyi adsorption potential (kJ/mol)
β_0,β_1	Descriptor coefficients for C_{50}
δ_0,δ_1	Descriptor coefficients for m

References

1. Wasilewska, M.; Derylo-Marczewska, A.; Marczewski, A.W. Comprehensive studies of adsorption equilibrium and kinetics for selected aromatic organic compounds on activated carbon. *Molecules* **2024**, *29*, 2038. [CrossRef] [PubMed]
2. Suhas; Kushwaha, S.; Chaudhary, M.; Chaudhary, S.; Tyagi, V.; Cansado, I.P.d.P.; Dehghani, M.H. Effect of substituent groups on the adsorption efficiency of phenols by activated carbon developed by hydrothermally treated Phyllanthus emblica fruit stone. *Toxics* **2024**, *12*, 874. [CrossRef] [PubMed]
3. Wasilewska, M.; Derylo-Marczewska, A.; Marczewski, A.W. Equilibrium and kinetic studies on adsorption of neutral and ionic species of organic adsorbates from aqueous solutions on activated carbon. *Molecules* **2024**, *29*, 3032. [CrossRef] [PubMed]
4. Vitek, R.; Masini, J.C. Nonlinear regression for treating adsorption isotherm data to characterize new sorbents: Advantages over linearization demonstrated with simulated and experimental data. *Heliyon* **2023**, *9*, e15128. [CrossRef] [PubMed]
5. Rajahmundry, G.K.; Garlapati, C.; Senthil Kumar, P.; Alwi, R.S.; Vo, D.-V.N. Statistical analysis of adsorption isotherm models and its appropriate selection. *Chemosphere* **2021**, *276*, 130176. [CrossRef] [PubMed]
6. Hamdaoui, O.; Naffrechoux, E. Modeling of adsorption isotherms of phenol and chlorophenols onto granular activated carbon. Part I. Two-parameter models and equations allowing determination of thermodynamic parameters. *J. Hazard. Mater.* **2007**, *147*, 381–394. [CrossRef] [PubMed]
7. Hamdaoui, O.; Naffrechoux, E. Modeling of adsorption isotherms of phenol and chlorophenols onto granular activated carbon. Part II. Models with more than two parameters. *J. Hazard. Mater.* **2007**, *147*, 401–411. [CrossRef] [PubMed]
8. Dubinin, M.M.; Radushkevich, L.V. The equation of the characteristic curve of activated charcoal. *Proc. Acad. Sci. USSR Phys. Chem. Sect.* **1947**, *55*, 331–337.
9. Dubinin, M.M. The potential theory of adsorption of gases and vapors for adsorbents with energetically non-uniform surfaces. *Chem. Rev.* **1960**, *60*, 235–241. [CrossRef]
10. Chu, K.H.; Hashim, M.A.; Bashiri, H.; Debord, J.; Harel, M.; Bollinger, J.-C. The Flory–Huggins isotherm and water contaminant adsorption: Debunking some modeling fallacies. *Ind. Eng. Chem. Res.* **2023**, *62*, 1121–1131. [CrossRef]
11. Harkins, W.D.; Jura, G. Surfaces of solids. XIII. A vapor adsorption method for the determination of the area of a solid without the assumption of a molecular area, and the areas occupied by nitrogen and other molecules on the surface of a solid. *J. Am. Chem. Soc.* **1944**, *66*, 1366–1373. [CrossRef]
12. Halsey, G. Physical adsorption on non-uniform surfaces. *J. Chem. Phys.* **1948**, *16*, 931–937. [CrossRef]
13. Henderson, S.M. A basic concept of equilibrium moisture. *Agric. Eng.* **1952**, *33*, 29–32.

14. Djaković Sekulić, T.; Jović, B.; Ivančev-Tumbas, I.; Panglisch, S. In silico modelling of selected organic substances adsorption from water onto activated carbon. *Chem. Eng. Sci.* **2024**, *287*, 119765. [CrossRef]
15. Ding, C.; Yuan, T.; Fu, R.; Xie, Y.; Shen, Z. Prediction and descriptor-level interpretation of organic pollutant adsorption by activated carbon using machine learning. *J. Environ. Chem. Eng.* **2026**, *14*, 123996. [CrossRef]
16. Mikolajczyk, A.P.; Fortela, D.L.B.; Berry, J.C.; Chirdon, W.M.; Hernandez, R.A.; Gang, D.D.; Zappi, M.E. Evaluating the Suitability of Linear and Nonlinear Regression Approaches for the Langmuir Adsorption Model as Applied toward Biomass-Based Adsorbents: Testing Residuals and Assessing Model Validity. *Langmuir* **2024**, *40*, 20428–20442. [CrossRef] [PubMed]
17. Serafin, J.; Dziejarski, B. Application of isotherms models and error functions in activated carbon CO_2 sorption processes. *Microporous Mesoporous Mater.* **2023**, *354*, 112513. [CrossRef]
18. Saeidi, N.; Vicente, D.J.; Chaudhuri, S.; Georgi, A. Modeling adsorption of mobile organic compounds on activated carbon and biochar using machine learning. *J. Environ. Chem. Eng.* **2026**, *14*, 123911. [CrossRef]
19. Allahkarami, E.; Dehghan Monfared, A.; Silva, L.F.O.; Dotto, G.L. Toward a mechanistic understanding of adsorption behavior of phenol onto a novel activated carbon composite. *Sci. Rep.* **2023**, *13*, 167. [CrossRef] [PubMed]
20. Marczewski, A.W.; Jaroniec, M. A new isotherm equation for single-solute adsorption from dilute solutions on energetically heterogeneous solids. *Monatsh. Chem.* **1983**, *114*, 711–715. [CrossRef]
21. Jaroniec, M.; Marczewski, A.W. Physical adsorption of gases on energetically heterogeneous solids. I. Generalized Langmuir equation and its energy distribution. *Monatsh. Chem.* **1984**, *115*, 997–1012. [CrossRef]
22. Marczewski, A.W.; Deryło-Marczewska, A.; Jaroniec, M. Correlations of heterogeneity parameters for single-solute and multi-solute adsorption from dilute solutions. *J. Chem. Soc. Faraday Trans. 1* **1988**, *84*, 2951–2957. [CrossRef]
23. Akaike, H. A new look at the statistical model identification. *IEEE Trans. Autom. Control* **1974**, *19*, 716–723. [CrossRef]
24. Burnham, K.P.; Anderson, D.R. *Model Selection and Multimodel Inference: A Practical Information-Theoretic Approach*, 2nd ed.; Springer: New York, NY, USA, 2002. [CrossRef]

Disclaimer/Publisher's Note: The statements, opinions and data contained in all publications are solely those of the individual author(s) and contributor(s) and not of MDPI and/or the editor(s). MDPI and/or the editor(s) disclaim responsibility for any injury to people or property resulting from any ideas, methods, instructions or products referred to in the content.